International Journal of QUANTUM CHEMISTRY

Computational Investigation of the Adsorption and Reactions of SiH_x ($x = 0$–4) on TiO_2 Anatase (101) and Rutile (110) Surfaces

Wen-Fei Huang,[a] Hsin-Tsung Chen,*[b] and M. C. Lin*[a]

The adsorption and reactions of the SiH_x ($x = 0$–4) on Titanium dioxide (TiO_2) anatase (101) and rutile (110) surfaces have been studied by using periodic density functional theory in conjunction with the projected augmented wave approach. It is found that SiH_x ($x = 0$–4) can form the monodentate, bidentate, or tridentate adsorbates, depending on the value of *x*. H coadsorption is found to reduce the stability of SiH_x adsorption. Hydrogen migration on the TiO_2 surfaces is also discussed for elucidation of the SiH_x decomposition mechanism. Comparing adsorption energies, energy barriers, and potential energy profiles on the two TiO_2 surfaces, the SiH_x decomposition can occur more readily on the rutile (110) surface than on the anatase (101) surface. The results may be used for kinetic simulation of Si thin-film deposition and quantum dot preparation on titania by chemical vapor deposition (CVD), plasma enhanced CVD, or catalytically enhanced CVD.

DOI: 10.1002/qua.24388

Introduction

Titanium dioxide (TiO_2) has become more attractive recently with numerous theoretical and experimental studies because of its promising applications in photocatalysts and photoelectrochemical processes.[1,2] The photophysics of TiO_2 sensitized by dyes,[3–5] polymers,[6,7] and semiconductors[8–10] have been widely investigated with an aim towards solar energy conversion by the photovoltaic effect. The dye-sensitized solar cells (DSSC) were invented by O'Regan and Grätzel (1991)[11] and the conversion efficiency of the DSSC have reached over 10%.[3–5,12,13] Organic dye molecules were attached onto the porous TiO_2 structures as adsorbate to provide an alternative photovoltaic device for electricity generation.[11,14] However, organic dyes are relatively expensive and less stable with shorter lifetimes than inorganic materials. Accordingly, many researchers[8–10] have attempted to use semiconductor quantum dots (QDs, such as InN, InP, InAs, PbS, and CdS) instead of dyes for solar cell applications. Wang and Lin[15] have successfully deposited the InN films on TiO_2 nanoparticle films by low-pressure organometallic chemical vapor deposition and found that the InN/TiO_2 films showed a broadband adsorption in the UV/visible range, covering 390–800 nm.

To improve the heterogeneous interface between a QD and TiO_2 and achieve higher efficiencies, there have been attempts to search for a variety of linkers (e.g., H_3BO_3,[16,17] BCl_x,[18] H_2S,[19] H_2O_2,[20] and HNO_3,[21]). An alternative material, the well-known silicon has been studied extensively for the solar cell applications.[22–31] Previously, the growth of Si on TiO_2 rutile (110) surface has been reported by Abad et al.[32] In addition, Lin et al.[33] have used SiH_4 as a precursor with Ar as a carrier gas to grow silicon QDs over a TiO_2 nanoparticle film by CVD. The Si QDs were protected by SiCx or SiNx thin films formed by CVD or plasma enhanced CVD (PECVD). The Si QDs distributed layer can generate electron-hole pairs to enhance the photon–electron transfer efficiency. The underlying physicochemical processes are very complex and it is hard to obtain the information on the detailed reaction mechanism under very limited experimental conditions. Accordingly, to improve our understanding of the complex Si-QDs growth process, we use the density functional theory (DFT) calculation to elucidate the reaction mechanism involved in the formation of the first layer Si film over the TiO_2 nanoparticle film.

In this article, we study the mechanisms for the decompositions of SiH_x on the two TiO_2 surfaces, anatase (101) and rutile (110), in relation to the potential growth of Si thin films and QDs, which may also be used as linkers for other QDs to attach on TiO_2. First, we study the adsorption energies and geometries of various SiH_x species with and without hydrogen coadsorption, useing DFT. The potential energy profiles of the reactions are calculated by nudged elastic band (NEB) method to be discussed below. The results of this study may help understand the SiH_x adsorption and decomposition mechanisms on the TiO_2 surface for fabrication of solar cells by CVD, PECVD, or catalytically enhanced CVD (Cat-CVD).

Computational Methods and Models

All calculations were performed by the spin-polarized DFT with the projected augmented wave method[34] as implemented in the Vienna *ab initio* simulation package.[35,36] The ionic cores were described by the generalized gradient approximation

[a] *W.-F. Huang, M. C. Lin*
Department of Applied Chemistry and Center of Interdisciplinary Molecular Science, National Chiao Tung University, Hsinchu 300, Taiwan
[b] *H.-T. Chen*
Department of Chemistry and Center for Nanotechnology, Chung Yuan Christian University, Chungli 32023, Taiwan
E-mail: htchen@cycu.edu.tw or chemmcl@emory.edu

with the PW91[37] formulation which has been shown to work well for gas-surface reactions.[16,21,38,39] The electronic orbitals were represented by the plane-wave expansion including all the plane waves with their kinetic energies smaller than the chosen cutoff energy, $\hbar k^2/2m < E_{cut}$, which ensures the convergence. The calculations were carried out with a 500 eV cutoff energy using the (4 × 4 × 4) and (3 × 3 × 1) Monkhorst–Pack *k*-points for the bulk and (101) surface of anatase, whereas the (2 × 4 × 2) and (4 × 3 × 1) Monkhorst–Pack *k*-points with the same cutoff energy were chosen for bulk and (110) surface of rutile, respectively. The NEB method[40] was applied to locate the transition states (TS). Two to eight images were used for each calculated TS. All the transition structures were verified by the frequency calculations. The adsorption energies were calculated by the following equation:

$$E_{ads} = -(E_{total} - E_{surf} - E_{gas})$$

where E_{total}, E_{surf}, and E_{gas} are the electronic energies of the adsorbed species on the surface, a clean TiO_2 surface, and a gas-phase molecule, respectively. In addition, we consider the Gibbs free energy, ΔG, of each gaseous species and their adsorption on the surfaces. The change of Gibbs free energy with finite temperature and pressure considered of the reaction can be calculated as follows:

$$\Delta G_{ads}(T,P) = E_{ads} - E_{surf} - E_{gas} + F^{vib,ads}(T) - [\Delta H_g(0K \rightarrow T, P^0) - TS_g(T,P^0) + kT\ln(p/P^0)]$$

where the Gibbs free energies of solid surface have relatively small variation with respect to temperature and pressure and are approximated by the DFT calculated total energy.

$$F^{vib}(T) = \sum_{i=1}^{n} F^{vib}(T,v_i) = \sum_{i=1}^{n}\left[\frac{hv_i}{2} + kT\ \ln(1-e^{-\beta hv_i})\right]$$

where $\beta = 1/kT$ and v_i is the vibration frequency. The total vibrational correction can be expressed as

$$F^{vib,ads}(T) = F^{vib}_{ads}(T) - F^{vib}_{g}(T)$$

where $F^{vib}_{ads}(T)$, $F^{vib}_{g}(T)$, and $F^{vib,ads}(T)$ are vibrational Gibbs free energies of the adsorbed molecule, the free gas molecule, and their change arising from the adsorbate-surface interaction, respectively.

The TiO_2 nanoparticle film is a polycrystalline material with different phases dependent on annealing temperature,[41–43] particle size,[44–46] and shape.[47] The rutile (110) and anatase (101) surfaces, which have the lowest surface energies with similar characteristics, may coexist in a nanoparticle film.[15,48] Theoretically, the (101)[49,50] and (110)[49] are the most stable surfaces of the anatase and rutile, respectively. Accordingly, both surfaces are considered in this calculation. The surface super cells are modeled as periodically repeated slabs each consisting of 24 units with three and four Ti layers for anatase and rutile, respectively, separated by a vacuum space greater than 13 Å, which guaranties no interactions between the slabs, for both surfaces as shown in Supporting Information Figure S1. The lower layers of each slab are fixed to preserve the calculated bulk parameters, whereas the remaining layers are fully relaxed to simulate the surface behavior during the calculations.

As shown in Supporting Information Figure S1, four different adsorption sites on both rutile (110) and anatase (101) surfaces are labeled. They are five-fold coordinated titanium, six-fold coordinated titanium, two-fold bridging oxygen, and three-fold coordinated oxygen, corresponding to Ti_{5c}, Ti_{6c}, O_{2c}, and O_{3c}, respectively. The coordinating unsaturated O_{2c} and Ti_{5c} sites are more active than the coordinating saturated O_{3c} and Ti_{5c} sites.[51,52] Gas-phase molecules are simulated in a cubic box with 20 Å on a side, which is large enough to ignore interactions between each periodic gas molecules.

To shorten the nomenclature, **H_xSi–y(a)** denotes SiH_x adsorption on the y site with the Si atom. For y, O represents an O_{2c} site and Ti represents a Ti_{5c} site. If three O adsorption sites coexist, the third O is an O_{3c} site. For example, **HSi–3O(a)** represents SiH adsorption on the O_{2c}, O_{2c}, and O_{3c} sites with the Si atom. Furthermore, **H_xSi–y, H(a)** denotes that **H_xSi–y(a)** coadsorbs with one hydrogen on an adjacent O_{2c} site, and **H_xSi–y…nH(a)** represents that SiH_x coadsorbs with n H atoms on the O_{2c} site at a long distance.

Results and Discussion

To verify the reliability of the computational results, we first compared the calculated bulk lattice constants with experimental values. The predicted lattice constants are $a = 3.824$ Å and $c = 9.678$ Å for anatase, which are in good agreement with the experimental values[53,54] of $a = 3.872$–3.875 Å and $c = 9.502$–9.514 Å, whereas those for rutile are $a = 4.593$ Å and $c = 2.958$ Å which are in reasonable agreement with the experimental values[53] of $a = 4.587$–4.593 Å and $c = 2.954$–2.959 Å. The predicted fractional coordinates (0.208 and 0.304 for the anatase and rutile bulk, respectively) also agree well with the experimental values (0.208[55] and 0.305[56]). The geometries of gas-phase molecules, $SiH_x(g)$ ($x = 1$–4), are also examined, and the results are summarized in Table S1 of the Supporting Information. Our results are in very good agreement with the experiment data.

Adsorption and reaction of SiH_x ($x = 0$–4) on the TiO_2 anatase (101) surface

Adsorption of SiH_x on the anatase (101) Surface. For each SiH_x adsorption on the TiO_2 anatase (101) surface, there are several possible configurations. SiH_x can adsorb at the O_{2c} or Ti_{5c} site to form a monodentate adsorbate, a bidentate adsorbate at the $(O_{2c})_2$ or $(O_{2c})(Ti_{5c})$ site, or a tridentate adsorbate at the $(O_{2c})_2(O_{3c})$ site, depending on the value of *x*. All the adsorption energies are listed in Table 1, and the geometries are shown in Figures 1, 4, and S2 of the Supporting Information. Figure 1 presents the geometries for the most stable configurations.

Table 1. Adsorption energies (kcal/mol) of SiH_4 fragments on the TiO_2 rutile (110) and TiO_2 anatase (101) surfaces with and without a coadsorbing H as depicted in the specified figures.

		On anatase surface				On rutile surface			
		With H—O_{2c}(a)[a]				With H—O_{2c}(a)[a]			
Adsorbate	Adsorption site	Figure	E_{ads}	Figure	E_{ads}	Figure	E_{ads}	Figure	E_{ads}
SiH_4	—O_{2c}	1a	1.2			5a	2.6		
SiH_3	—O_{2c}	1b	57.6	4b	53.4	5b	76.1	8b	68.4
	—Ti_{5c}	S2a	2.2	S2b	17.7	S7a	11.8	S7b	20.7
SiH_2	—O_{2c}	4e	38.6	4d	36.7	8e	50.5	8d	40.7
	—O_{2c}, —Ti_{5c}	S2c	50.6	S2d	50.3				
	—O_{2c}, —O_{2c}	1c	90.6	S2e	85.7	5c	103.2	S7c	79.1
SiH	—O_{2c}	S2f	52.0	S2g	51.8	S7d	69.5	S7e	64.3
	—O_{2c}, —Ti_{5c}	S2h	52.1	S2i	45.6				
	—O_{2c}, —O_{2c}	4i	81.2	4h	78.2	8k	87.8	8j	75.4
	—O_{2c}, —O_{2c}, —O_{3c}	1d,4n	108.6, 98.5	S2j, S2k	96.7, 91.3	5d	125.8	S7f	109.8
Si	—O_{2c}	S2l	61.0	S2m	56.2	S7g	79.0	S7h	65.4
	—O_{2c}, —Ti_{5c}	S2n	66.0	S2o	61.9				
	—O_{2c}, —O_{2c}	S2p	90.4	S2q	84.4	S7i	110.4	S7j	96.2
	—O_{2c}, —O_{2c}, —O_{3c}	1e, 4q	100.5, 91.3	4l, 4p	93.9, 83.8	5e	113.4	8p	100.8

[a] With hydrogen coadsorption on an adjacent O_{2c} site.

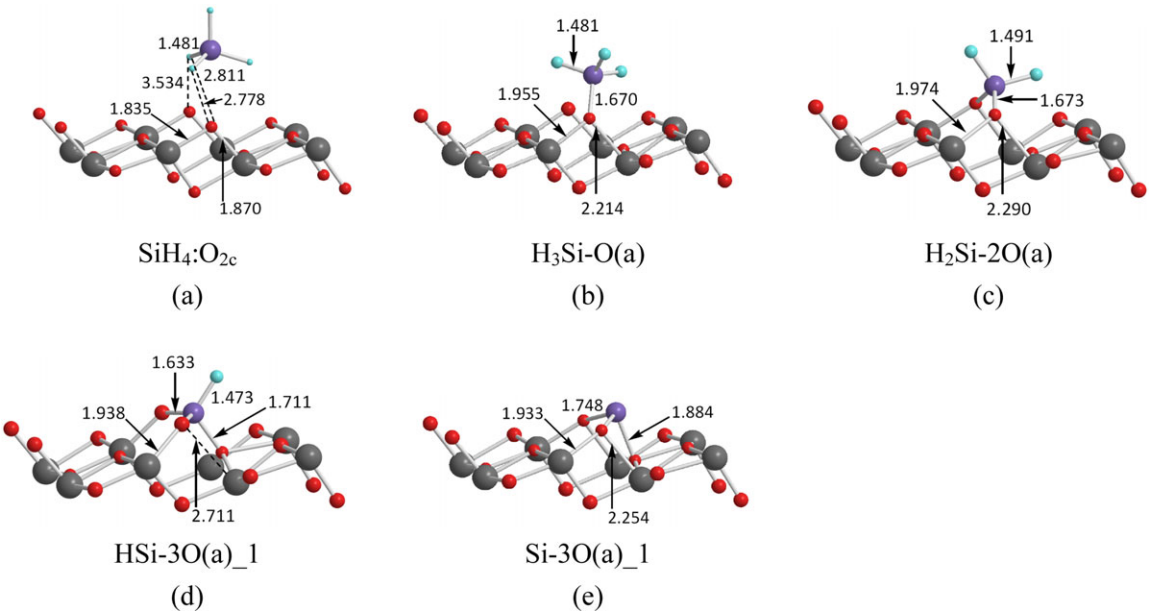

Figure 1. The optimized geometries of adsorbed SiH_4 and its fragments, SiH_3, SiH_2, SiH, and Si, on the TiO_2 anatase (101) surface. [Color figure can be viewed in the online issue, which is available at wileyonlinelibrary.com.]

The other geometries involved in the potential energy profiles (discussed in the next section) are shown in Figure 4, and the remaining ones are shown in Supporting Information Figure S2. The adsorption free energies of most stable SiH_4 fragments on the TiO_2 rutile (110) and TiO_2 anatase (101) Surfaces at the temperature of 298, 400, 600, and 1000 K, respectively, are calculated and listed in Table 2.

As shown in Figure 1, SiH_4 molecule can interact with an O_{2c} atom of the anatase surface by physisorption, using its H atoms. The lengths of H…O_{2c} are 2.778, 2.811, and 3.534 Å. Its adsorption energy is calculated to be 1.2 kcal/mol; see Table 1. To carry out mechanistic studies, we examined the adsorption sites and energies for SiH_3, SiH_2, SiH, and Si as well. The most stable configuration for SiH_3 adsorption is located at an O_{2c} site with an adsorption energy of 57.6 kcal/mol. The bond length of Si—O_{2c} is 1.670 Å. On the contrary, the SiH_3 only weakly bonds with a Ti_{5c} site with a small adsorption energy of 2.2 kcal/mol. For the SiH_2 adsorption, the most stable configuration is located at the O_{2c}, O_{2c} bridging site (**H_2Si–2O(a)**). The **H_2Si–2O(a)** has an adsorption energy of 90.6 kcal/mol and the Si atom is bound to two O anions of the surface with Si—O distances of 1.673 Å. In addition, the formation of the Si—O bonds produces much relaxation of the surface O anion bonded to the silicon atom, resulting in the protrusion by approximately 0.42 Å from the surface. The monodentate adsorption at the O_{2c} site (**H_2Si–O(a)**) and bidentate

Table 2. Adsorption free energies (kcal/mol) of the most stable SiH_4 fragments on the TiO_2 rutile (110) and TiO_2 anatase (101) surfaces with and without a coadsorbing H.

		On anatase surface				On rutile surface			
		With H—O_{2c}(a)[a]				With H—O_{2c}(a)[a]			
Adsorbate	Temperature (K)	Figure	ΔG_{ads}	Figure	ΔG_{ads}	Figure	ΔG_{ads}	Figure	ΔG_{ads}
SiH_4	298	1a	−7.8	–	–	5a	−6.4	–	–
	400		−9.7		–		−8.3		–
	600		−14.1		–		−12.7		–
	1000		−22.2		–		−20.8		–
SiH_3	298	1b	45.4	4b	41.2	5b	63.9	8b	56.2
	400		42.5		38.3		61.0		53.3
	600		35.7		31.5		54.2		46.5
	1000		22.6		18.4		41.1		33.4
SiH_2	298	1c	76.0	S2e	71.1	5c	88.6	S7c	64.5
	400		72.8		67.9		85.4		61.3
	600		65.5		60.6		78.1		54.0
	1000		51.4		46.5		64.0		39.9
SiH	298	1d	95.6	S2j	83.7	5d	112.8	S7f	96.8
	400		92.3		80.4		109.5		93.5
	600		85.2		73.3		102.4		86.4
	1000		71.4		59.5		88.6		72.6
Si	298	1e	92.6	4l	86.0	5e	105.5	8p	92.9
	400		90.1		83.5		103.0		90.4
	600		85.0		78.4		97.9		85.3
	1000		75.0		68.4		87.9		75.3

[a] With hydrogen coadsorption on an adjacent O_{2c} site.

adsorption at the O_{2c}, Ti_{5c} sites (**H_2Si–OT(a)**) are less stable (see Table 1). For SiH and Si adsorption, five different configurations on different sites of the anatase surface are found. Different from SiH_2, the SiH and Si preferentially adsorb on two O_{2c} and one O_{3c} anions of the surface, forming **HSi–3O(a)_1** (Fig. 1d), **HSi–3O(a)_2** (Fig. 4n) and **Si–3O(a)_1** (Fig. 1e), **Si–3O(a)_2** (Fig. 4q), respectively. As shown in Table 1, the **HSi–3O(a)_1** and **Si–3O(a)_1** are more stable than H**Si–3O(a)_2** and **Si–3O(a)_2**. The adsorption energy of **HSi–3O(a)_1** is 108.6 kcal/mol and the Si—O_{2c} and Si—O_{3c} distances are 1.633 and 1.711 Å, respectively. While the corresponding values for **Si–3O(a)_1** are 100.5 kcal/mol and 1.748 and 1.884 Å, respectively.

In addition, we also consider the SiH_x and H coadsorption. Their optimized structures are depicted in Figure 4 and Figure S2 of the Supporting Information. As summarized in Table 1, the adsorption energy with hydrogen attaching to a neighboring oxygen site decreases in the range of 0.2–11.9 kcal/mol. These results indicate that the hydrogen coadsorption may destabilize the SiH_x adsorption on the TiO_2 anatase (101) surface, unlike the enhancement effects of H-coadsorption on the binding of OH,[57,58] HS,[19] NO_3,[21] and $HOBO_2$[16] species with titania.

Reaction of SiH_x on the anatase (101) Surface. *Hydrogen Migration and H_2 Desorption.* The decomposition reaction of SiH_4 can be schematically expressed by the following mechanism:

$$\begin{aligned} H_4Si(a) &\rightarrow H_3Si(a) + H - O_{2c}(a) \rightarrow H_2Si(a) + 2H - O_{2c}(a) \\ &\rightarrow \ldots\ldots \rightarrow Si(a) + 4H - O_{2c}(a) \end{aligned} \quad (1)$$

The dissociated H atoms can adsorb on adjacent O_{2c} sites to potentially block active sites and thus stop the subsequent decomposition reactions. Accordingly, the migration of H atoms has been studied first. Here, we only consider the hydrogen adsorption on the O_{2c} site, **H–O_{2c}(a)** because the adsorption energy of H on the O_{2c} site (56.1 kcal/mol) is more stable than that on the Ti_{5c} site (0.7 kcal/mol).

It is readily understandable that the distribution of hydrogen adsorption sites will affect the transition state energy barriers strongly. To solve this problem, we consider one of the Si—H bonds of SiH_x firstly decomposes to a nearest O_{2c} site, and then migrates to an adjacent O_{2c} site. The hydrogen atom can effectively "jump" on adjacent O_{2c} sites away from SiH_x for it to undergo further decomposition. The scheme is shown in Supporting Information Figure S3. As depicted in Figure 2, one hydrogen adsorbs on the $^{\#1}O_{2c}$ site can migrate along two directions, one along $< \bar{1}11 >$ to the $^{\#2}O_{2c}$ site and another one along $< 010 >$ to the $^{\#4}O_{2c}$ site. The hydrogen can migrate to the $^{\#2}O_{2c}$ site by overcoming **TS2a** with 13.1 kcal/mol. The migration to the $^{\#4}O_{2c}$ site is achieved by a stepwise reaction. The hydrogen moves to the $^{\#3}O_{2c}$ site with an endothermicity of 15.4 kcal/mol via **TS2b** (26.7 kcal/mol), and then continues moving to the $^{\#4}O_{2c}$ site with an exothermicity of 15.4 via **TS2c** (11.7 kcal/mol). In conclusion, the hydrogen migration is easier along the $< \bar{1}11 >$ than the $< 010 >$ direction.

The other possible reactions are also considered; two hydrogen atoms adsorbed at two neighboring O_{2c} sites may recombine to give one H_2 gas molecule, which is another possible reaction to vacate adjacent O_{2c} sites. As shown in Figure 2b, the energy barrier (**TS2d**) for forming H_2(g) is 43.2 kcal/mol,

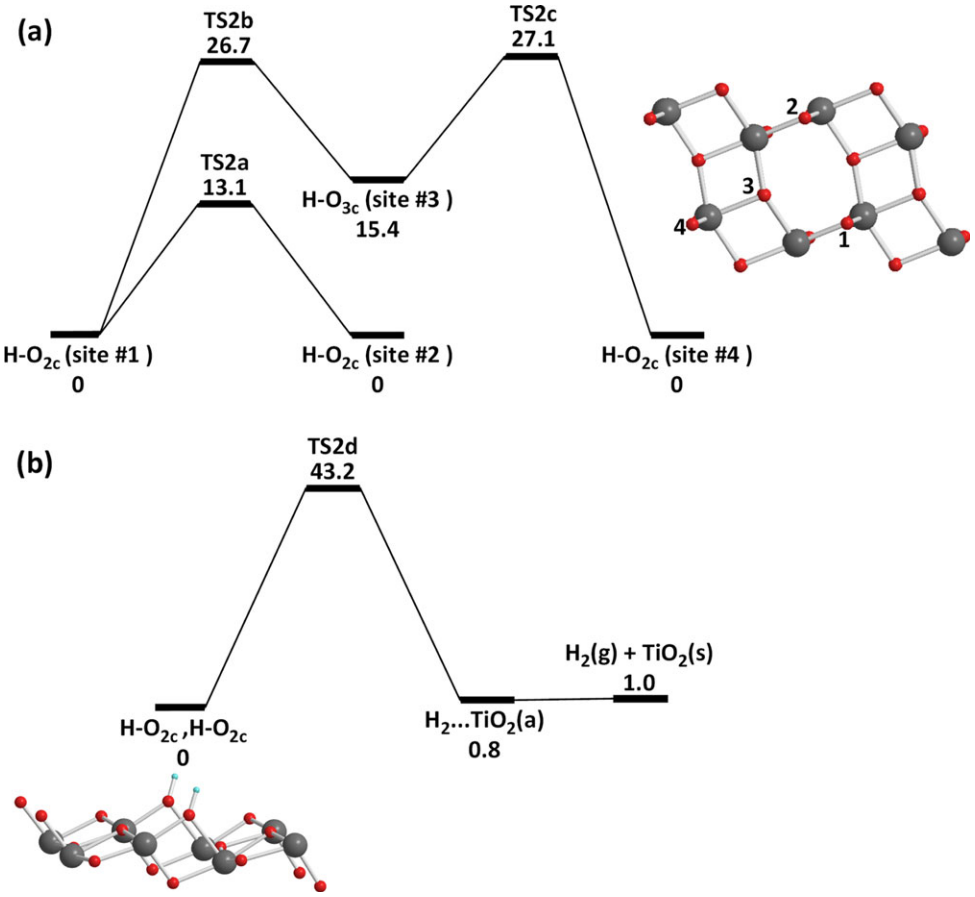

Figure 2. Schematic potential energy profiles for a) the H migration and b) the H_2(g) formation on the TiO_2 anatase (101) surface. [Color figure can be viewed in the online issue, which is available at wileyonlinelibrary.com.]

which is much higher than the energy barrier (**TS2a**, 13.1 kcal/mol) of the lowest hydrogen migration path. Hence, hydrogen atom migration is considered as the main process for vacating two adjacent O_{2c} sites by the SiH_x adsorbate. Other possible reaction paths for forming H_2(g), for example, H—O_{2c},H—O_{2c}(a) –> H_2–O_{2c}(a) –> H_2(g) + TiO_2(s), are also considered; however, all the energy barriers involved are higher than **TS2d** of 43.2 kcal/mol.

SiH_x Decomposition. Figure 3 shows the schematic potential energy profiles for the multipath on the TiO_2 anatase (101) surface, and the related decomposition energy barriers and reactions energies are listed in Table 3. As seen in Figure 3a, the reaction starts from the SiH_4 adsorption at an O_{2c} site, denoted by **SiH_4:O_{2c}** (Fig. 1a), with an exothermicity of 1.2 kcal/mol. The SiH_4 decomposition can be realized by breaking one of the Si—H bonds with an energy barrier (**TS3a**) of 22.1 kcal/mol. The dissociating H atom primarily attaches to an adjacent bridging O_{2c} anion forming an O—H bond of 0.978 Å and co-adsorbs with SiH_3, producing **H_3Si–O,H(a)** (Fig. 4b) with an exothermicity of 15.4 kcal/mol. The coadsorbing hydrogen in **H_3Si–O,H(a)** can jump along the nearest O_{2c} site to a long distance, producing **H_3Si–O…H(a)**, with an exothermicity of 4.2 kcal/mol.

As shown in Table 4, the energy barriers of hydrogen migration on the anatase (101) surface with different coexisting adsorbates differ only by 0.4–0.5 kcal/mol. Therefore, we can consider all the energy barriers between **H_xSi–O,H(a)** and **H_xSi–O…H(a)** to be approximately 13.1 kcal/mol. The dissociation energy for SiH_4(g) –> SiH_3(g) + H(g) is 90.4 kcal/mol,[59] which is much larger than the energy barrier at **TS3a**, 20.9 kcal/mol, for SiH_4 decomposition on the anatase (101) surface as one would expect.

As shown in Figure 3b, the second decomposition process takes place by overcoming a 44.1 kcal/mol reaction barrier at **TS3b**, producing hydrogen coadsorbed **H_2Si–O,H(a)** with an endothermicity of 39.6 kcal/mol. The Si…H distance is 3.653 Å in **H_2Si–O,H(a)** (Fig. 4d), in which the coadsorbates, SiH_2 and H, interact weakly, hence the energy difference between **H_2Si–O,H(a)** and **H_2Si–O…H(a)** is only 1.9 kcal/mol. The SiH_2 radical can adsorb on the surface with monodentate and bidentate configurations; therefore, three possible reaction paths are also considered as follows:

$$H_2Si-O(a) \rightarrow HSi-O...H(a) \rightarrow Si-O...2H(a) \quad (2)$$

$$\rightarrow H_2Si-OT(a) \rightarrow HSi-OT...H(a) \rightarrow Si-OT...2H(a) \quad (3)$$

$$\rightarrow H_2Si-2O(a) \rightarrow HSi-3O...H(a) \rightarrow Si-3O...2H(a) \quad (4)$$

The related potential energy profiles are shown in Figure 3 and Supporting Information Figure S4. The path (4), named multipath, is the most likely reaction pathway due to the most

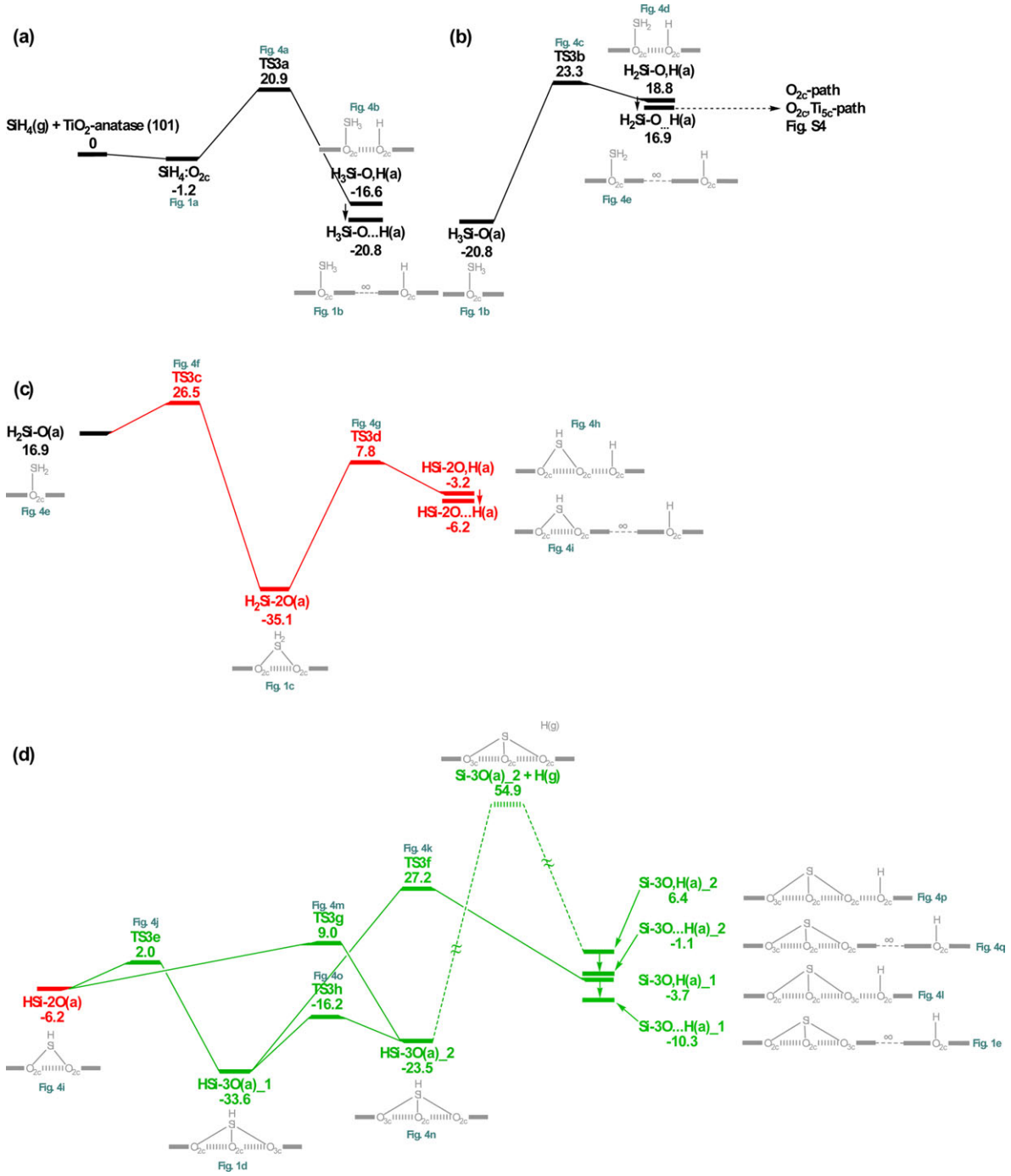

Figure 3. Schematic potential energy profiles for the multipath on the TiO_2 anatase (101) surface. The detail geometries are shown in Figure 4, and the referring adsorption energies are shown in Table 1. (For brevity, in Figs. 3b, 3c, and 3d, one, two, and three H(a) co-adsorptions are, respectively, omitted although they are included in the energy calculations. Hence, the reactant **H_3Si–O(a)** represents **H_3Si–O**…**H(a)** and **H_2Si–O(a)** denotes **H_2Si–O**…**2H(a)**). [Color figure can be viewed in the online issue, which is available at wileyonlinelibrary.com.]

stable intermediates and the smaller energy barriers involved. The paths (2) and (3), named O_{2c}-path and O_{2c},Ti_{5c}-path, respectively, are less important; they are shown in Supporting Information Figure S4. In the following, we only discuss the most likely reaction pathway (4).

As illustrated in Figure 3c, the SiH_2 bound at the two O_{2c} sites, **H_2Si–2O(a)** (Fig. 1c), can be formed from **H_2Si–O(a)** by overcoming an energy barrier (**TS3c**) of 9.6 kcal/mol with an

Table 3. The decomposition energy barriers and the reaction energies for $SiH_x(a) \rightarrow SiH_{x-1}$...H(a) (unit: kcal/mol).

		$x = 4$	$x = 3$	$x = 2$	$x = 1$
On anatase	Energy barrier	20.9	44.1	26.5	33.4
	Reaction energy	−20.8	37.7	−23.1	−4.1
On rutile	Energy barrier	28.8	38.6	22.9	28.7
	Reaction energy	−43.0	27.4	−24.0	−24.7

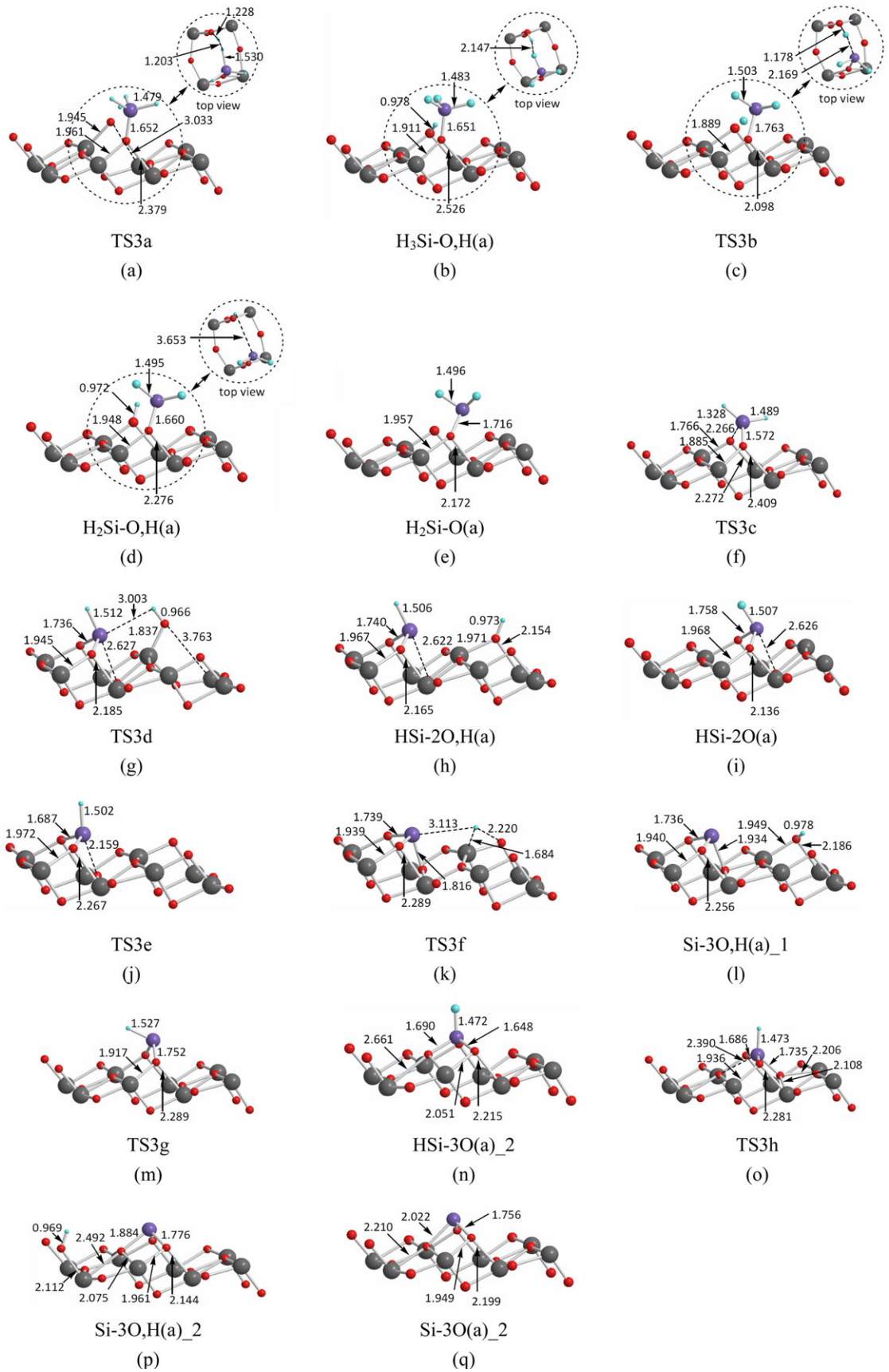

Figure 4. The optimized geometries along the multipath on the TiO_2 anatase (101) surface. [Color figure can be viewed in the online issue, which is available at wileyonlinelibrary.com.]

Table 4. Energy barriers (kcal/mol) of H migration affected by adjacent adsorbates.

	None	SiH_3	SiH_2	SiH
On anatase	13.1	12.7	13.6	12.7
On rutile	31.1	28.3	28.3	27.6

exothermicity of 52.0 kcal/mol. Comparing with the formation of another intermediate, **H_2Si–OT(a)** (Supporting Information Fig. S2c), **TS3c** is 2.6 kcal/mol higher than **TSs3** (Supporting Information Fig. S4) because the O_{2c}…O_{2c} distance (3.823 Å) is larger than the O_{2c}…Ti_{5c} distance (1.839 Å). However, **H_2Si–2O(a)** is 40 kcal/mol more stable than **H_2Si–OT(a)**, and the Si—O_{2c} bond length (1.673 Å) in **H_2Si–2O(a)** is shorter than the Si—O_{2c} and Si—Ti_{5c} bond lengths (1.685 and 2.522 Å) in **H_2Si–OT(a)**. Overcoming a 42.9 kcal/mol energy barrier at **TS3d**, one of the H—Si bonds of **H_2Si–2O(a)** can dissociate to the adjacent O_{2c} site to form the coadsorption **HSi–2O,H(a)** (Fig. 4h) with an endothermicity of 31.9 kcal/mol. The **HSi–2O(a) adsorbate** (Fig. 4i) can be formed with 3.0 kcal/mol exothermicity from the **HSi–2O,H(a)** by H migration. The tridentate adsorbate, **HSi–3O(a)_1** is formed from the bidentate adsorbate, **HSi–2O(a)**, by passing over **TS3e** with an exothermicity of 27.4 kcal/mol, as shown in Figure 3d. The Si—O_{3c} bond (1.711 Å) is 0.078 Å longer than Si—O_{2c} bond (1.633 Å) in **HSi–3O(a)_1** due to the coordination with the saturated O_{3c} site. The H-migration from **HSi–3O(a)_1** producing **Si–3O,H(a)_1** (Fig. 4l) with an endothermicity of 29.9 kcal/mol via **TS3f** has a high barrier of 60.8 kcal/mol. The coadsorbed hydrogen can move from the **Si–3O,H(a)_1** configuration to produce the single Si adsorption, **Si–3O(a)_1** (Fig. 1e), with an exothermicity of 6.6 kcal/mol. By overcoming **TS3g** with a 15.2 kcal/mol barrier, the bidentate adsorbate, **HSi–2O(a)**, also can bond with another O_{3c} site to form **HSi–3O(a)_2** (Fig. 4n) with an exothermicity of 17.3 kcal/mol. The tridentate adsorbate, **HSi–3O(a)_2**, is 10.1 kcal/mol less stable than **HSi–3O(a)_1**. Different from **HSi–3O(a)_1**, the dehydrogenation of **HSi–3O(a)_2** has a very high barrier of 78.4 kcal/mol because the distance of H to the closest O_{2c} site in **HSi–3O(a)_2** (5.175 Å) is too long for hydrogen dissociation. However, the **HSi–3O(a)_2** can isomerize to the **HSi–3O(a)_1** by passing through an energy barrier of only 17.4 kcal/mol (**TS3h**).

The mechanisms for the dehydrogenation process, H_xSi–O,H(a) –> H_2(g) + H_{x-1}Si–O(a) for x = 1–3, are also considered for SiH_x decomposition. The energy barriers for x = 1–3 are calculated to be 45.3, 33.9, and 52.8 kcal/mol, respectively, which are much higher than the energy barrier of hydrogen migration (**TS2a**, 13.1 kcal/mol). The potential energy profiles for these three reaction paths are shown in Figure S6 of the Supporting Information. Obviously, the reaction paths of H_xSi–O,H(a) –> H_2(g) + H_{x-1}Si–O(a) are less likely to take place than those of H_xSi–O,H(a) –> H_xSi–O…H(a) –> H_{x-1}Si–O,H…H(a) –> H_{x-1}Si-O…2H(a), due to their higher energy barriers.

Adsorption and reaction of SiH_x (x = 0–4) on the TiO_2 rutile (110) surface

Adsorption of SiH_x on the rutile (110) Surface. Figure 5 shows the geometries for the most stable configurations on the rutile (110) surface. The other geometries involving in the potential energy profiles (discussed in the next section) are shown in Figure 8, and the remaining ones are shown in Supporting Information Figure S7.

Similar to the results on the anatase (101) surface, the SiH_4 molecule physisorbs on the rutile (110) surface with an adsorption energy of 2.6 kcal/mol, and the most stable configurations for each SiH_x are **H_3Si–O(a)**, **H_2Si–2O(a)**, **HSi–3O(a)**, and **Si–3O(a),** with their corresponding adsorption energies: 76.1, 103.2, 125.8, and 113.4 kcal/mol. Comparing with the results on the anatase (101) surface, the SiH_x adsorbates on the rutile surface are bound more strongly with higher energies by 6.6–20.0 kcal/mol. Notably, the **H_xSi–OT(a)** structures

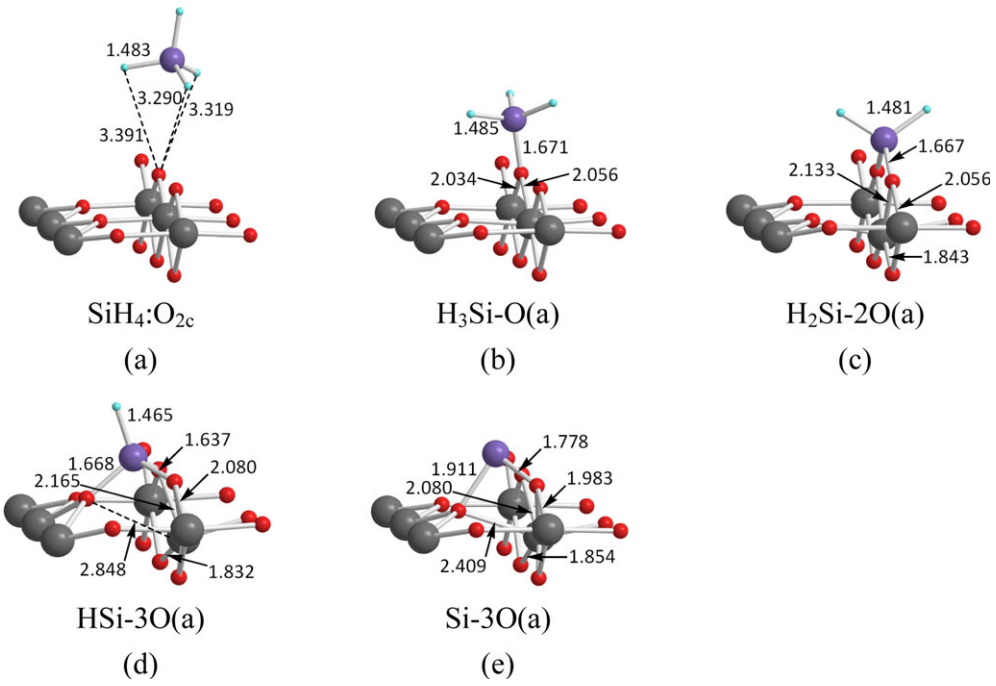

Figure 5. The optimized geometries of adsorbed SiH_4 and its fragments, SiH_3, SiH_2, SiH, and Si, on the TiO_2 rutile (110) surface. [Color figure can be viewed in the online issue, which is available at wileyonlinelibrary.com.]

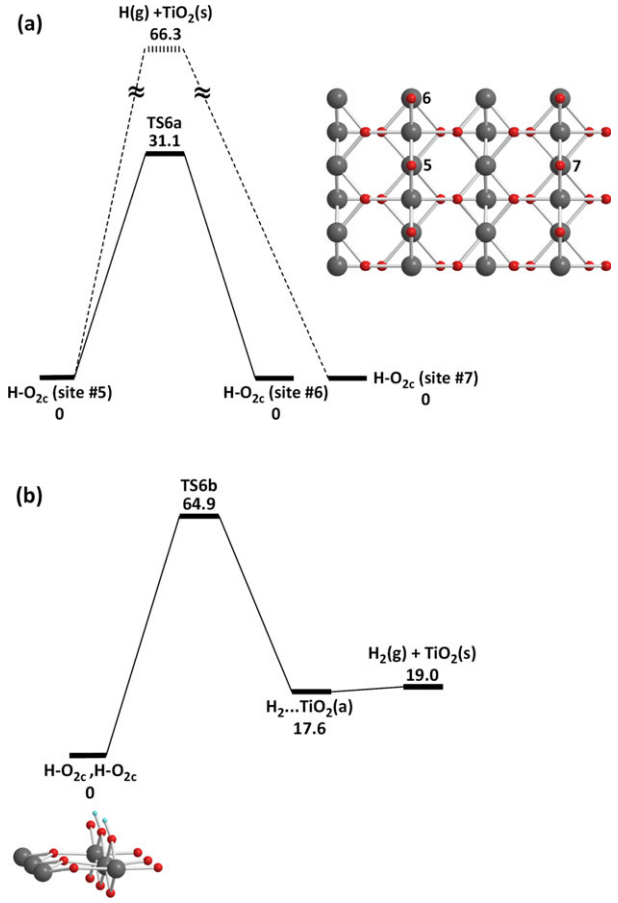

Figure 6. Schematic potential energy profiles for a) the H migration and b) the H_2(g) formation on the TiO_2 rutile (110) surface. [Color figure can be viewed in the online issue, which is available at wileyonlinelibrary.com.]

cannot be formed on the rutile (110) surface because of the different topography.

The SiH_x and H coadsorption is also considered here, and the optimized structures are depicted in Figure 8 and Figure S7 of the Supporting Information. Similar to the results on the anatase (101) surface, the H coadsorption destabilizes the SiH_x adsorption. The decreases in adsorption energies by H coadsorption are in the range of 5.2–24.1 kcal/mol, which are more significant than those on the anatase (101) surface.

Reaction of SiH_x on the rutile (110) Surface. *Hydrogen Migration.* Similar to the results on the anatase (101) surface, the hydrogen adsorption at the O_{2c} site (66.3 kcal/mol) is more stable than that at the Ti_{5c} site (1.6 kcal/mol). Hence, we also consider hydrogen migration on the rutile (110) surface to understand the SiH_x decomposition on the surface. As shown in Figure 6, one hydrogen at $^{\#5}O_{2c}$ site can migrate along two directions on the rutile (110) surface, one along $<001>$ to the $^{\#6}O_{2c}$ site and another one along $<\bar{1}10>$ to the $^{\#7}O_{2c}$ site. To realize the migration along the $<\bar{1}11>$ direction, we double the size of the surface model in the $<\bar{1}11>$ direction. As shown in Figure 6, the hydrogen migrates to the $^{\#6}O_{2c}$ site with a 31.1 kcal/mol barrier at **TS6a**. However, the long distance (6.586 Å) between $^{\#5}O_{2c}$ and $^{\#7}O_{2c}$ increases the difficult for migration along the $<\bar{1}11>$ direction. Hence, the only possible direction for hydrogen migration is along the $<001>$ direction. Comparing to the anatase (101) surface, hydrogen migration occurs less easily on the rutile (110) surface due to the lower energy barrier for the former process (13.1 vs. 31.1 kcal/mol). Hence, the SiH_x ($x = 1$–4) stepwise decomposition may be easier on the anatase (101) surface due to the vacating of the nearest O_{2c} site by hydrogen migration.

Similar to the anatase case, the reactions of H_2(g) formation cannot compete with the hydrogen migration reactions. As shown in Figure 6b, the energy barrier (**TS6b**) for H_2(g) production is predicted to be 64.9 kcal/mol, which is much higher than the energy barrier (**TS6a**, 31.1 kcal/mol) of the lowest hydrogen migration path.

SiH_x Decomposition. Similar to the reactions on the TiO_2 anatase (101) surface, the reactions of SiH_x on the TiO_2 rutile (110) surface can be divided into two paths: O_{2c}-path and multipath. However, the O_{2c}, Ti_{5c}-path does not exist on the rutile (110) surface since the **H_xSi–OT(a)** configuration does not exist. The multipath shown in Figure 7 is the main path in the rutile case, and the structures involved are shown in Figure 8. The related decomposition energy barriers and reaction energies are listed in Table 3. The O_{2c}-path is the less important reaction path, as shown in Figure S8 of the Supporting Information.

Similar to the reactions on the anatase surface, the first step of the reactions on the TiO_2 rutile (110) surface is the SiH_4 physisorbed on the O_{2c} site, named **SiH_4:O_{2c}** (Fig. 5a), with an exothermicity of 2.6 kcal/mol as alluded to above. By overcoming an energy barrier of 31.4 kcal/mol from **SiH_4:O_{2c}** via **TS7a**, **H_3Si–O,H(a)** (see Fig. 8b structure) can be formed exothermically by 32.7 kcal/mol. The migration of the H atom from the O_{2c} site in **H_3Si–O,H(a)** producing **H_3Si–O…H(a)** is exothermic by 7.7 kcal/mol. As shown in Figure 7b, the **H_2Si–O,H(a)** (see Fig. 8d structure) can be formed endothermically with 37.3 kcal/mol by breaking an H—Si bond in **H_3Si–O(a)** via **TS7b** (38.6 kcal/mol). The **H_2Si–O…H(a)** can be formed by hydrogenation migration in **H_2Si–O,H(a)** with an exothermicity of 9.9 kcal/mol. The H—Si—H line of the bonds is along $<\bar{1}10>$ direction in **H_2Si–O,H(a)**. The SiH_2 molecule rotates in concurrent with the hydrogen migration.

The bidentate adsorbate, **H_2Si–2O(a)**, can be formed from the monodentate adsorbate, **H_2Si–O(a)**, by overcoming a very small bending barrier of 0.9 kcal/mol at **TS7c** with a large exothermicity of 52.7 kcal/mol attributable to the formation of a new bond. Different from the case on the anatase (101) surface, the formation of **HSi–3O(a)** on the rutile (110) surface is a stepwise path. The migration of one of the H atoms in **H_2Si–2O(a)** may be accomplished by forming the intermediate **M8a** (see Fig. 8h structure) first with a large endothermicity of 46.8 kcal/mol via **TS7d** by overcoming a very high barrier of 73.3 kcal/mol. Comparing with the energy for hydrogen dissociation from **H_2Si–2O(a)** producing HSi–2O(a) + H(g) (95.0 kcal/mol), the transition state **TS7d** is 21.7 kcal/mol lower in energy as one would expect. Overcoming **TS7e** with a barrier of 28.8 kcal/mol, the H on the O_{2c} site in **M8a** can migrate to the closest O_{2c} site forming **HSi–2O,H(a)** (see Fig. 8j structure), with an

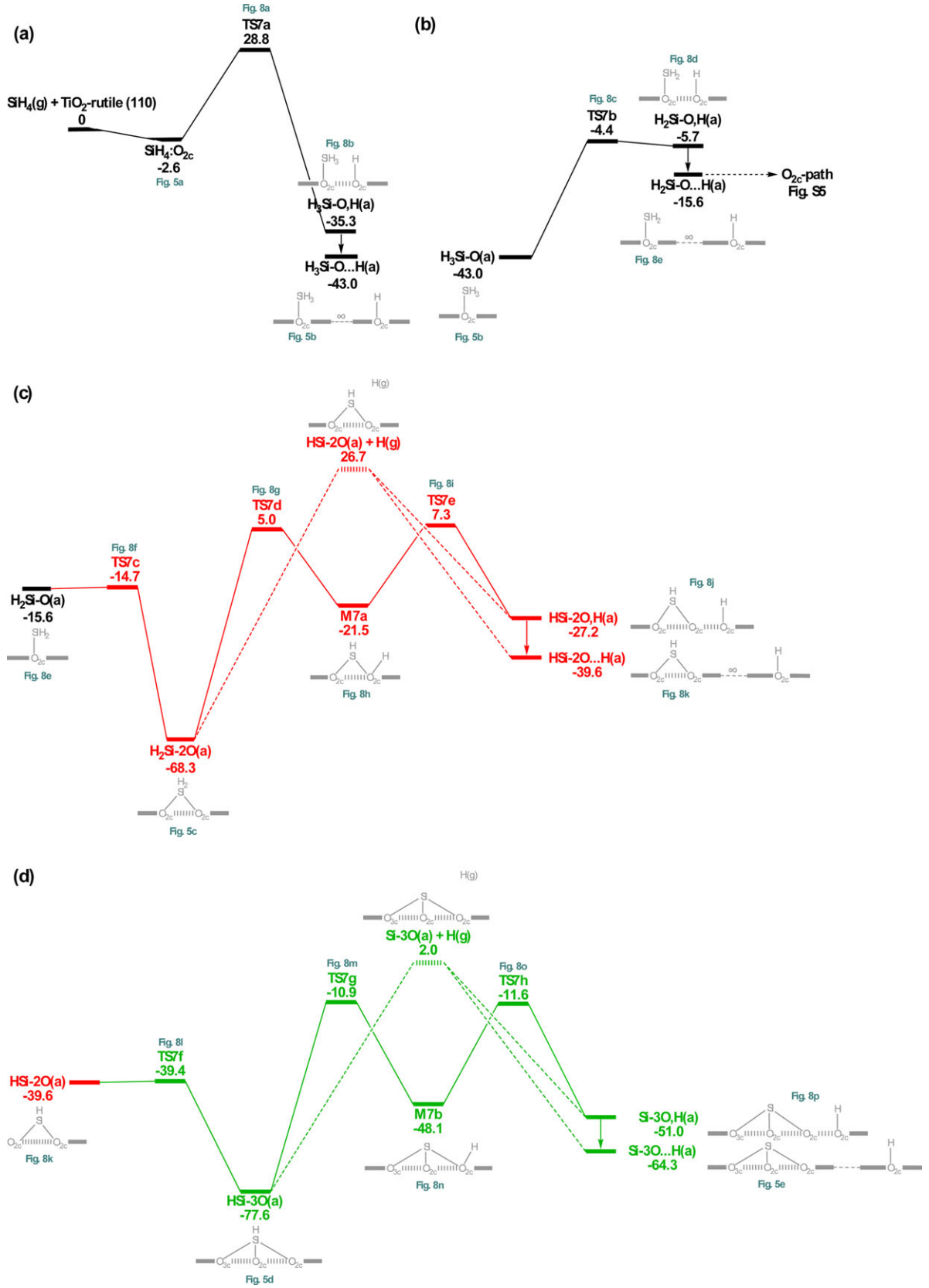

Figure 7. Schematic potential energy profiles for the multipath on the TiO_2 rutile (110) surface. The detail geometries are shown in Figure 8, and the referring adsorption energies are shown in Table 1. (For brevity, in Figs. 7b, 7c, and 7d, one, two, and three H(a) co-adsorptions are, respectively, omitted although they are included in the energy calculations. Hence, the reactant **H_3Si–O(a)** represents **H_3Si–O**…**H(a)** and **H_2Si–O(a)** denotes **H_2Si–O**…**2H(a)** here.) [Color figure can be viewed in the online issue, which is available at wileyonlinelibrary.com.]

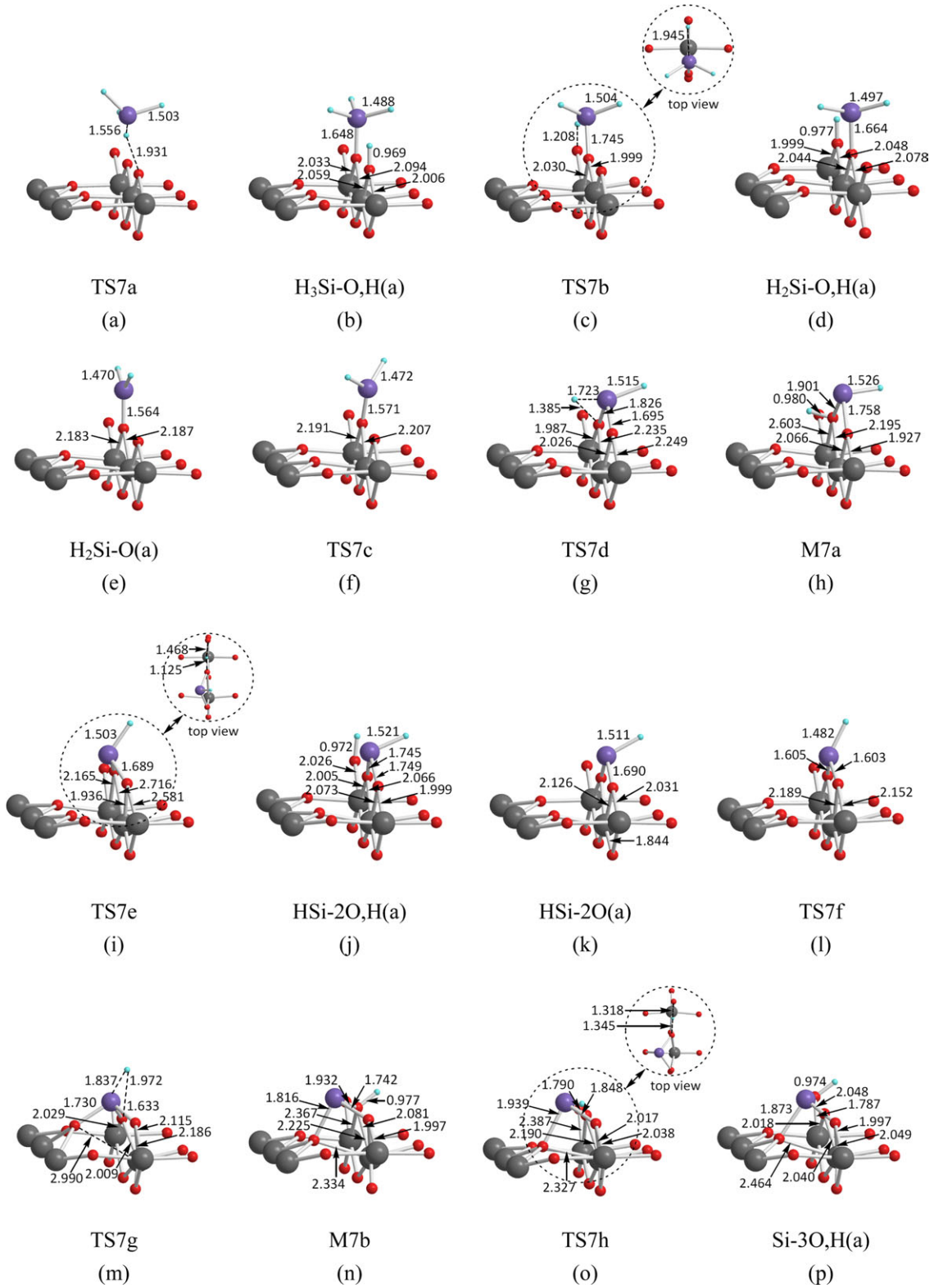

Figure 8. The optimized geometries along the multipath on the TiO_2 rutile (110) surface. [Color figure can be viewed in the online issue, which is available at wileyonlinelibrary.com.]

exothermicity of 5.7 kcal/mol. The migration of the detached H atom from the Si atom in **HSi–2O,H(a)** producing **HSi–2O…H(a)** (see Fig. 8k structure) is exothermic by 12.4 kcal/mol.

Similar to the case on the anatase (101) surface, the **HSi–2O(a)** can adsorb on the surface with a tridentate configuration forming the **HSi–3O(a)** (see Fig. 4d structure) with an exothermicity of 38.0 kcal/mol via **TS7f** having a small bending

barrier of 0.2 kcal/mol. The O_{2c}—Ti_{6c} bond of **HSi–3O(a)** is almost broken with a long distance of 2.848 Å. Similar to the case of **H_2Si–2O(a)**, hydrogen migration from **HSi–3O(a)** can occur by a stepwise pathway. First, the hydrogen migrates to the O_{2c} site, which binds with the SiH molecule, forming **M8b** (see Fig. 8n structure) with an endothermicity of 29.5 kcal/mol via **TS7g** by overcoming a large barrier of 66.7 kcal/mol. For **HSi–3O(a)**, the direct hydrogen dissociation into the gas-phase occurs with an endothermicity of 79.6 kcal/mol, which is higher than **TS7g**. Overcoming an energy barrier of 36.5 kcal/mol via **TS7h**, the hydrogen of **M8b** can migrate to the closest O_{2c} site with an exothermicity of 2.9 kcal/mol, forming **Si–3O,H(a)** (see Fig. 8p structure). The hydrogen migration process from **Si–3O,H(a)** produces the tridentate adsorbate, **Si–3O**…**H(a)** (see Fig. 5e structure), with an exothermicity of 13.3 kcal/mol.

Similar to the anatase case, the mechanisms for the dehydrogenation reactions, H_xSi–O,H(a) –> H_2(g) + $H_{x-1}Si$–O(a) for x = 1–3, are also considered. The energy barriers for x = 1–3 are 48.6, 14.3, and 51.4 kcal/mol, respectively; see Figure S10 of the Supporting Information. Similar to the anatase case, the reactions for H_2(g) formation cannot compete with the hydrogen migration reactions due to their higher energy barriers.

Comparing with the results on the anatase (101) surface, the energy barriers of the **H_2Si–O(a)** –> **H_2Si–2O(a)** and **HSi–2O(a)** –> **HSi–3O(a)** processes on the rutile surface are higher by 11 kcal/mol on average. Conversely, the intermediates and products are more stable on the rutile surface than those on the anatase surface with much larger exothermicities of 42 kcal/mol on average (see Figs. 3 and 7).

The reaction energies for SiH_x dissociation reactions in the gas phase are known as follows:[59]

$$\mathrm{SiH_4(g) \rightarrow SiH_3(g) + H(g)} \quad \Delta E = 90.4\ \mathrm{kcal/mol}$$
$$\mathrm{SiH_3(g) \rightarrow SiH_2(g) + H(g)} \quad \Delta E = 68.1\ \mathrm{kcal/mol}$$
$$\mathrm{SiH_2(g) \rightarrow SiH(g) + H(g)} \quad \Delta E = 73.6\ \mathrm{kcal/mol}$$
$$\mathrm{SiH(g) \rightarrow Si(g) + H(g)} \quad \Delta E = 72.8\ \mathrm{kcal/mol}$$

These energies are significantly higher than the barriers for their dissociation reactions on the two titania surfaces according to the potential energy profiles depicted in Figures 3 and 7, reflecting the catalytic effects of the TiO_2 surfaces which may help the growth of Si thin films and QDs upon annealing.

Conclusions

The mechanisms for SiH_x decomposition on the two TiO_2 surfaces, anatase (101) and rutile (110), have been investigated by periodic DFT calculations. Our results show that SiH_4 physisorbs weakly on the two surfaces, whereas the SiH_3 preferentially adsorbs at an O_{2c} site with monodentate configuration. SiH_2 binds strongly at two O_{2c} sites with a bidentate configuration and SiH and Si adsorb more favorably at the $(O_{2c})_2(O_{3c})$ sites with tridentate configurations. Their adsorption energies are predicted to be 1.2, 57.6, 90.6, 108.6, and 100.5 kcal/mol on the anatase (101) surface and 2.6, 76.1, 103.2, 125.8, and 113.4 kcal/mol on the rutile (110) surface, respectively. Hydrogen coadsorption with these species was found to reduce the stability of SiH_x adsorption, contrary to the known electron withdrawing groups such as OH and SH, among others. Hydrogen migration on the TiO_2 surfaces has also been studied in conjunction with SiH_x decomposition. We find that hydrogen migration is easier on the anatase (101) surface. In addition, the potential energy surfaces for the reactions of SiH_x on the two TiO_2 surfaces have been constructed. The stable intermediates on the two surfaces are bidentate adsorbates, **H_2Si–2O(a)**, with binding energies >90 kcal/mol and tridentate adsorbates, **HSi–3O(a)** and **Si–3O(a)**, with binding energies >100 kcal/mol. Comparing the adsorption energies on the two TiO_2 surfaces, the SiH_x species bind more strongly on the rutile (110) surface by as much as 42 kcal/mol on average, whereas the barriers for their decomposition reactions are higher than those on the anatase surface by 11 kcal/mol on average. The results of this study may be used, for example, for kinetic simulations of Si thin-film deposition and QD growth upon annealing on titania by CVD, PECVD, or Cat-CVD.

Acknowledgments

The authors are grateful to Taiwan's National Center for High-performance Computing for the CPU's facility and to Taiwan National Science Council under Grant Numbers NSC 101-2113-M-033-009-MY3 and NSC 101-2632-M-033-001-MY2 for the research support. MCL also wants to acknowledge Taiwan Semiconductor Manufacturing Co. for the TSMC Distinguished Professorship and Taiwan National Science Council for the Distinguished Visiting Professorship at the Center for Interdisciplinary Molecular Science, National Chiao Tung University, Hsinchu, Taiwan.

Keywords: titanium dioxide · gas-surface reactions · SiH_x decomposition · density functional theory

How to cite this article: W.-F. Huang, H.-T. Chen, M. C. Lin, *Int. J. Quantum Chem.* **2013,** *113*, 1696–1708. DOI: 10.1002/qua.24388

Additional Supporting Information may be found in the online version of this article.

[1] K. I. Hadjiivanov, D. G. Klissurski, *Chem. Soc. Rev.* **1996**, *25,* 61.
[2] A. L. Linsebigler, G. Lu, J. T. Yates, *Chem. Rev.* **1995**, *94,* 735.
[3] M. Gratzel, *Nature* **2001**, *414,* 338.
[4] M. K. Nazeeruddin, A. Kay, I. Rodicio, R. Humphry-Baker, E. Muller, P. Liska, N. Vlachopoulos, M. Gratzel, *J. Am .Chem. Soc.* **1993**, *115,* 6382.
[5] B. O'Regan, M. Gratzel, *Nature* **1991**, *353,* 737.
[6] C. L. Huisman, A. Goossens, J. Schoonman, *Chem. Mater.* **2003**, *15,* 4617.
[7] D. Li, C. Gu, C. Guo, C. Hu, *Chem. Phys. Lett.* **2004**, *385,* 55.
[8] P. Yu, K. Zhu, A. G. Norman, S. Ferrere, A. J. Frank, A. J. Nozik, *J. Phys. Chem. B* **2006**, *110,* 25451.
[9] J. L. Blackburn, D. C. Celmarten, A. J. Nozik, *J. Phys. Chem. B* **2003**, *107,* 14154.
[10] R. Vogel, P. Hoyer, H. Weller, *J. Phys. Chem.* **1994**, *98,* 3183.
[11] B. O'Regan, M. Grätzel, *Nature* **1991**, *353,* 737.

[12] A. Yella, H. -W. Lee, H. N. Tsao, C. Yi, A. K. Chandiran, M. K. Nazeeruddin, E. W. -G. Diau, C. -Y. Yeh, S. M. Zakeeruddin, M. Grätzel, *Science* **2011**, *334,* 629.
[13] C. Chen, M. Wang, J. Li, N. Pootrakulchote, L. Alibabaei, C. Ngoc-le, J. Decoppet, J. Tsai, C. Grätzel, C. Wu, S. Zakeeruddin, M. Grätzel, *ACS Nano* **2009**, *3,* 3103.
[14] W. R. Duncan, O. V. Prezhdo, *Annu. Rev. Phys. Chem.* **2007**, *58,* 143.
[15] J. -H. Wang, M. C. Lin, *ChemPhysChem.* **2004**, *5,* 1615.
[16] P. Raghunath, M. C. Lin, *J. Phys. Chem. C* **2008**, *112,* 8276.
[17] P. Raghunath, M. C. Lin, *J. Phys. Chem. C* **2009**, *113,* 3751.
[18] J. -G. Chang, J. -H. Wang, M. C. Lin, *J. Phys. Chem. A* **2007**, *111,* 6746.
[19] W. -F. Huang, H. -T. Chen, M. C. Lin, *J. Phys. Chem. C* **2009**, *113,* 20411.
[20] H. Wen-Fei, P. Raghunath, M. C. Lin, *J. Comput. Chem.* **2011**, *32,* 1065.
[21] C. -Y. Chang, H. -T. Chen, M. C. Lin, *J. Phys. Chem. C* **2009**, *113,* 6140.
[22] A. Shah, P. Torres, R. Tscharner, N. Wyrsch, H. Keppner, *Science* **1999**, *285,* 692.
[23] R. B. Bergmann, *Appl. Phys. A* **1999**, *69,* 187.
[24] L. Stalmans, J. Poortmans, H. Bender, M. Caymax, K. Said, E. Vazsonyi, J. Nijs, R. Mertens, *Prog. Photovolt. Res. Appl.* **1998**, *6,* 233.
[25] B. Hamilton, *Semicond. Sci. Technol.* **1995**, *10,* 1187.
[26] R. L. Smith, S. D. Collins, *J. Appl. Phys.* **1992**, *71,* R1.
[27] A. G. Cullis, L. T. Canham, P. D. J. Calcott, *J. Appl. Phys.* **1997**, *82,* 909.
[28] P. R. McCurdy, L. J. Sturgess, S. Kohli, E. R. Fisher, *Appl. Surf. Sci.* **2004**, *233,* 69.
[29] V. G. Erkov, S. F. Devyatova, E. L. Molodstova, T. V. Malsteva, U. A. Yanovskii, *Appl. Surf. Sci.* **2000**, *166,* 51.
[30] P. G. Karlesson, J. H. Richter, M. P. Andersson, J. Blomquist, H. Siegbahn, P. Uvdal, A. Sandell, *Surf. Sci.* **2005**, *580,* 207.
[31] S. Takabayashi, R. Nakamura, Y. Nakato, *J. Photochem. Photobiol. A* **2004**, *166,* 107.
[32] J. Abad, C. Rogero, J. Méndez, M. F. López, J. A. Martín-Gago, E. Román, *Appl. Surf. Sci.* **2004**, *234,* 497.
[33] M. C. Lin, T. -N. Yang, S. -M. Lan, T. -Y. Wei, J. -P. Chiu, W. Y. Ma, Method of fabricating silicon quantum dots-sensitized layer of silicon quantum dots-sensitized solar cells, Issued/Publication Date: 2007/09/01; Patent Number: 200733406; IPC: H01L-031/042(200601), Taiwan.
[34] P. Blochl, *Phys. Rev. B* **1994**, *17,* 953.
[35] G. Kresse, J. Furthmuller, *J. Comput. Mater. Sci.* **1996**, *6,* 15.
[36] G. Kresse, J. Furthmuller, *Phys. Rev. B* **1996**, *54,* 11169.
[37] J. P. Perdew, Y. Wang, *Phys. Rev. B* **1992**, *45,* 13244.
[38] J. -H. Wang, M. C. Lin, *J. Phys. Chem. B* **2006**, *110,* 2263.
[39] J. -H. Wang, M. C. Lin, Y. -C. Sun, *J. Phys. Chem. B* **2005**, *109,* 5133.
[40] G. Mills, H. Jonsson, G. K. Schenter, *Surf. Sci.* **1995**, *324,* 305.
[41] K. D. Kim, S. H. Kim, H. T. Kim, *Colloids Surf.* **2005**, *254,* 99.
[42] G. L. Li, G. H. Wang, *Nanostruct. Mater.* **1999**, *11,* 663.
[43] Y. Hwu, Y. D. Yao, N. F. Cheng, C. Y. Tung, H. M. Lin, *Nanostruct. Mater.* **1997**, *9,* 355.
[44] H. Zhang, J. F. Banfield, *J. Mater. Chem.* **1998**, *8,* 2073.
[45] H. Zhang, J. F. Banfield, *J. Phys. Chem. B* **2000**, *104,* 3481.
[46] M. R. Ranade, A. Navrotsky, H. Z. Zhang, J. F. Banfield, S. H. Elder, A. Zaban, P. H. Borse, S. K. Kulkarni, G. S. Doran, H. J. Whitfield, *Proc. Natl. Acad. Sci.* **2002**, *99,* 6476.
[47] A. N. Enyashin, G. Seifert, *Phys. Status Solidi B* **2005**, *242,* 1361.
[48] W. Li, C. Ni, H. Lin, C. P. Huang, S. I. Shah, *J. Appl. Phys.* **2004**, *96,* 6663.
[49] F. Labat, P. Baranek, C. Adamo, *J. Chem. Theory Comput.* **2008**, *4,* 341.
[50] M. Lazzeri, A. Vittadini, A. Selloni, *Phys. Rev. B* **2001**, *63,* 155409.
[51] A. Vittadini, A. Selloni, F. P. Rotzinger, M. Gratzel, *Phys. Rev. Lett.* **1998**, *81,* 2954.
[52] M. Ramamoorthy, D. Vanderbilt, R. D. King-Smith, *Phys. Rev. B* **1994**, *49,* 16721.
[53] J. K. Burdett, T. Hughbanks, G. J. Miller, J. W. Richardson, Jr., J. V. Smith, *J. Am. Chem. Soc.* **1987**, *109,* 3639.
[54] C. J. Howard, T. M. Sabine, F. Dickson, *Acta Cryst.* **1991**, *47,* 462.
[55] M. Horn, C. F. Schwerdtfeger, E. P. Meagher, *Z. Kristallogr.* **1972**, *136,* 273.
[56] H. Perron, J. Vandenborre, C. Domain, R. Drot, J. Roques, E. Simoni, J. -J. Ehrhardt, H. Catalette, *Surf. Sci.* **2005**, *72,* 518.
[57] J. Zhao, B. Li, K. D. Jordan, J. Yang, H. Petek, *Phys. Rev. B* **2006**, *73,* 195309.
[58] K. Onda, B. Li, J. Zhao, K. D. Jordan, J. Yang, H. Petek, *Science* **2005**, *308,* 1154.
[59] NIST Computational Chemistry Comparison and Benchmark Database, NIST Standard Reference Database Number 101, Release 15b, August 2011, Editor: Russell D. Johnson III, Available at: http://cccbdb.nist.gov/

Received: 14 October 2012
Revised: 11 December 2012
Accepted: 17 December 2012
Published online on 8 January 2013